Design, Manufacturing and Assembly of the STORT Hypersonic Flight Experiment Thermal Protection System

Thomas Reimer[1], Giuseppe D. Di Martino[2], Ivaylo Petkov[3], Lucas Dauth[4] and Luis Baier[5]
DLR Institute of Structures and Design, Stuttgart, 70569, Germany

Ali Gülhan[6] and Florian Klingenberg[7]
DLR Institute of Aerodynamics and Flow Technology, Cologne, 51147, Germany

Dorian Hargarten[8]
DLR Space Operations and Astronaut Training, Wessling, 82234, Germany

STORT is a DLR project focused on testing of key technologies for flight at hypersonic Mach numbers of higher than 8 for a relatively long time. The overarching aim of the project is to support cost reduction of future space transportation systems while at the same time keeping them highly reliable. To this end, reusability of all stages of future launcher systems is a prerequisite. For first stages, a Mach number of 8-10 seems to be the optimum staging velocity, which means that technologies for the return flight of first stages at those speeds need to be developed and validated. Consequently, STORT aimed at achieving operating conditions representative of such high-energetic reentry flights for reusable first stages at Mach 8, to support the optimization and validation of technologies and simulation tools for the development of future space transportation systems. The present paper thus describes the design, manufacturing and integration of the rocket forebody assembly up to the launch of the vehicle. In addition, an overview of the collected flight data from the thermal protection system sensors is given. The forebody thermal protection system requires the use of ceramic matrix composite material for protection from the high heat loads experienced during the flight. In the present case the thermal protection system was constituted by C/C-SiC composite structures built in-house by DLR. The main elements were a conical nose element and four thin-walled shell segments manufactured via filament winding of carbon fibers. Via an in-situ joining process, integral fixation brackets from CMC material were permanently attached to the shells. The underlying forebody main structure to which the thermal protection system structures were connected was made from aluminum.

[1] Research Engineer, Space Systems Integration, Pfaffenwaldring 38-40
[2] Research Engineer, Space Systems Integration.
[3] Research Engineer, Space Systems Integration.
[4] Research Engineer, Ceramic Matrix Composites.
[5] Research Engineer, Ceramic Matrix Composites.
[6] Department Head, Supersonic and Hypersonic Technologies, STORT Project Manager
[7] Research Engineer, Supersonic and Hypersonic Technologies.
[8] Research Engineer, Mobile Rocket Base (MORABA).

I. Introduction

The purely simulation-based design of future space transportation systems via numerical tools is a long-term goal of DLR's research programs. Since ground testing facilities are limited in replicating the flight environment, real flight data is of great importance to validate and calibrate the tools. Sounding rocket flight experiments are a cost-efficient way to collect high-quality in-flight data, both for compensating the deficits of ground experimental testing and for providing valuable data for the definition and validation of reliable numerical tools.

To this end, the German Aerospace Center (DLR) has carried out several projects over recent years on the design and construction of sounding rocket flight experiments with the twofold objective of collecting relevant flight data and demonstrating technologies for reusable launcher first stages. While previous and other ongoing DLR projects for flight experiments focus on short-term high-speed flight [1] and aerodynamics and control at Mach numbers lower than 5 [2, 3], the focus of the STORT project is on the thermo-mechanical challenges encountered by highly thermally stressed components at high Mach numbers (higher than 8) for a relatively long time, of approximately 2 minutes [4]. This allows to increase the integral thermal load, thus obtaining more representative conditions of high-energetic re-entry flights for application in reusable first or even upper stages.

In this framework, the DLR Institute of Structures and Design with the two departments RSI (Space System Integration) and KVS (Ceramic Matrix Composites) was responsible for the design, manufacture, assembly and testing of the forebody of the launcher for the flight experiment. Because the CMC external structures were subjected to high heat loads and mechanical loads during the flight, they had to be made of ceramic matrix composite (CMC) materials and the design process had to consider a challenging thermo-mechanical environment.

II. System Overview and Flight Plan

Previous flight experiments as SHEFEX II did reach high speed of Mach 10 towards the end of the re-entry phase, but the duration of the aerothermal load was just about 30 seconds and the temperatures of the structures were not going up to very high values due to the capacitive effects of the structures. For STORT it was the objective to achieve high aerothermal loads for a longer time and to reach higher temperatures on the TPS structures as a consequence of the longer flight duration in the aerothermal load environment. Typical sounding rocket flight experiments as the currently ongoing REFEX project are based on a two-stage rocket motor combination using for instance the brazilian S31/S30 type. However, with the envisaged payload mass of 200 kg the achievable velocity using this motor combination is limited to Mach 5-6. Therefore, it was decided to design a three-stage flight experiment using the S31 as first stage, the S30 as second stage and to put an Improved Orion (IO) as third stage on top. In addition to the use of a third stage, specific push-down maneuvers were implemented in the flight plan to follow a so-called suppressed trajectory with corresponding high integral thermal loads.

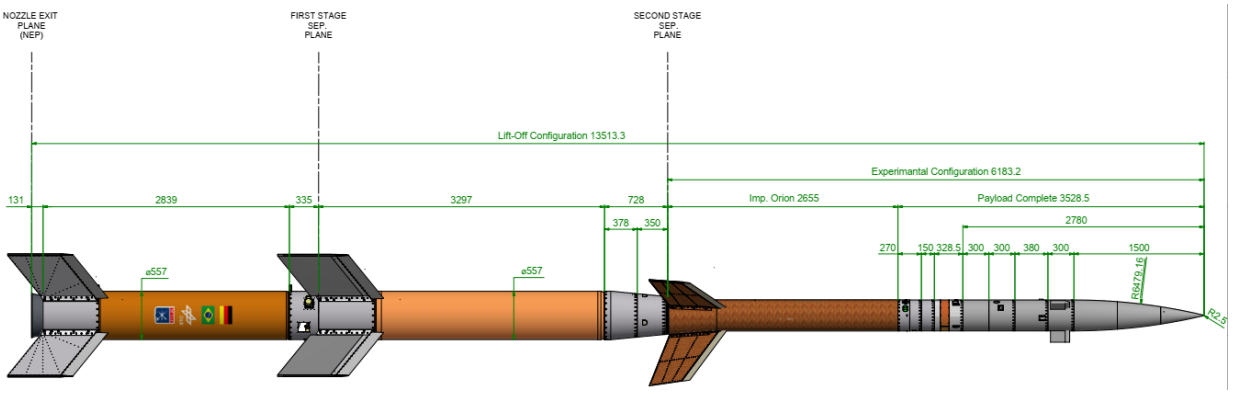

Fig. 1 STORT launch vehicle.

The full stack of the flight configuration is shown in Fig. 1. The total launch vehicle length was 13.51 m. The lenghtes of the S31, S30 and IO (inc. payload) were 3.31 m, 4.02 m and 6.17 m, respectively. On top of the IO motor, the payload was installed with a total length of 3.53 m and a total mass of 200 kg. The payload consisted of several modules of specific functions and the so-called forebody which featured an outer surface fully made of CMC. The stack of modules on top of the IO motor is shown in Fig. 2. They included the service module, the cork-coated CFRP hybrid module, the data acquisition module, the coolant gas storage module and the canard module. Finally, in the very front of the payload unit, the CMC forebody was situated.

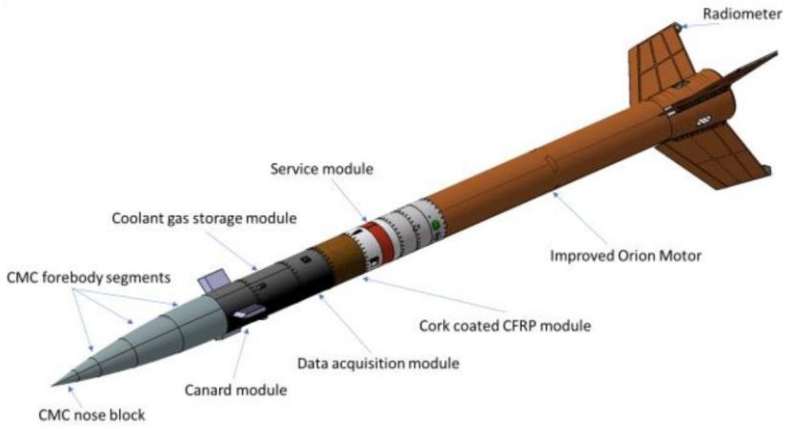

Fig. 2 STORT third stage (IO) with CMC forebody and integrated experiment and service modules [4].

The altitude and Mach number profiles for the flight are shown in Fig. 3. As shown in Fig. 3 it was planned to fly at a Mach number of 8 for almost two minutes which was only possible due to the use of the third stage. Between the burn-out of the first stage and the ignition of the second stage, a gravity turn was carried out to adjust the pointing direction of the unguided remaining second/third stage combination to a lower flight path angle. The same type of maneuver was done before third stage ignition. As a result, the Mach number could be increased from 4 to 8 during the third stage firing while the altitude increase after the burn-out of the second stage to the apogee altitude of 38 km was only about 8 km.

The S31 first stage and the S30 second stage motors are actively separated during ascent, however, after the burn-out of the third stage IO motor there is no separation from the payload unit but they stay connected. The IO motor acts as the stabilisator for the payload forebody during the experiment phase in the downleg of the flight.

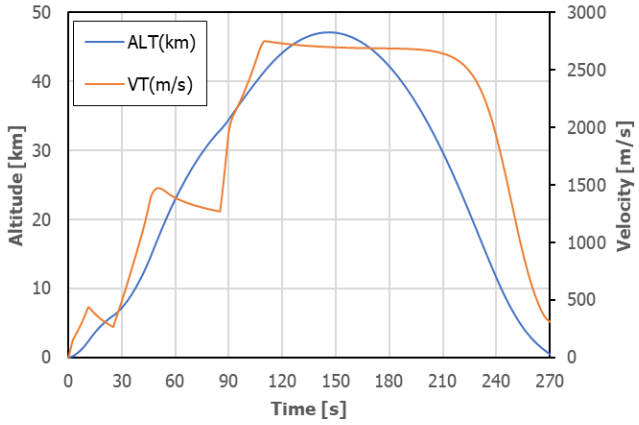

Fig. 3 STORT flight experiment nominal trajectory.

III. STORT Forebody Structure

Since the flight experiment was specifically designed to replicate high aerothermal loads for a longer duration, it was clear that a TPS is required and that the temperatures in the front of the vehicle would rise to considerable values. Therefore, the forebody of the launch vehicle was designed to feature a surface consisting fully of CMC material, to demonstrate to a certain degree the technology for longer-duration hypersonic flight. The third stage with the CMC forebody of 1.5 m length is depicted in Fig. 4.

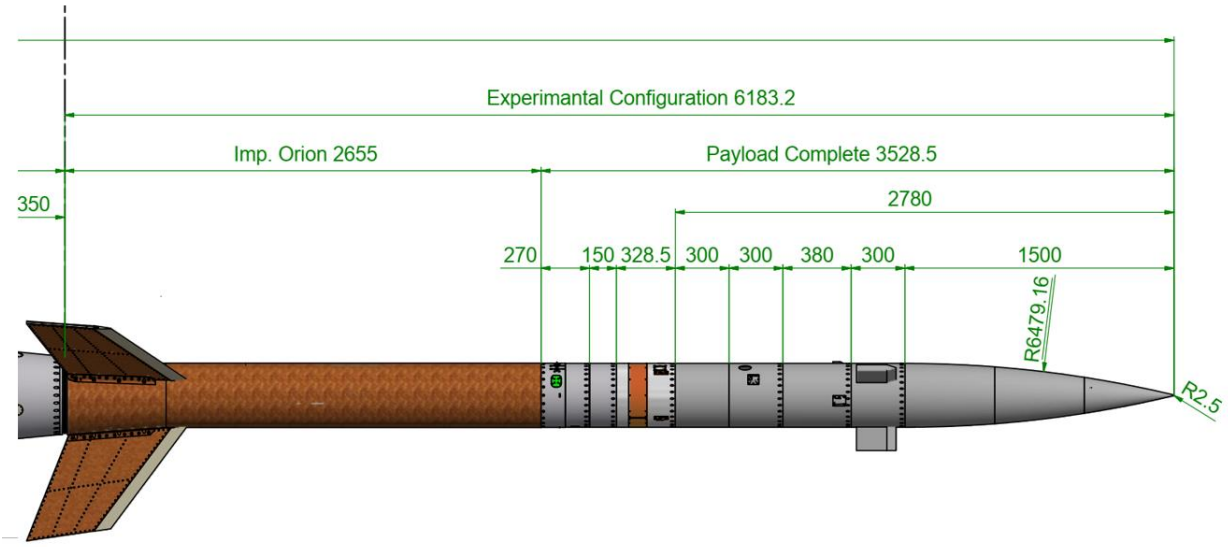

Fig. 4 STORT third stage overview.

The main requirement for the design process was to obtain a smooth external surface, which would allow to investigate the aerodynamic phenomena typical of hypersonic flows. Thus, the goal was to reduce disturbances in the surface, like gaps, to the minimum. As a result, in order to reduce the number of parts, the forebody CMC structures were designed as circumferentially closed axially symmetric thin-walled structures, named segments A-D, produced via filament winding. An internal metallic strucure made from aluminium was designed to install the CMC TPS structures around it. One solid nose tip also made from CMC material was on the very tip of the vehicle.

The TPS structures of the launcher forebody consisted of the in-house manufactured C/C-SiC material, which is a carbon fiber-reinforced ceramic. The material is produced via the Reactive Melt Infiltration (RMI) process; also referred to as the Liquid Silicon Infiltration (LSI) process, specifically for this material. The fibers are carbon fibers, the matrix is a mix of amorphous carbon in the fiber bundle blocks surrounded by silicon carbide and small amounts of residual silicon [5].

The shell segments were manufactured via wet filament winding of the carbon fibers with a polymeric resin and subsequent pyrolysis and liquid silicon infiltration. In addition, the in-situ joining method [6], developed also in-house, was implemented to attach CMC brackets to the main shells on the inside. In this way, the shells could be connected to the metallic understructure, avoiding rivets or bolted connections on the outside which would have affected the external aerodynamic flow. Fig. 5 shows a section view of the forebody structure overall model. Overlapping interface geometries between the segments were designed to avoid open gaps on the TPS surface.

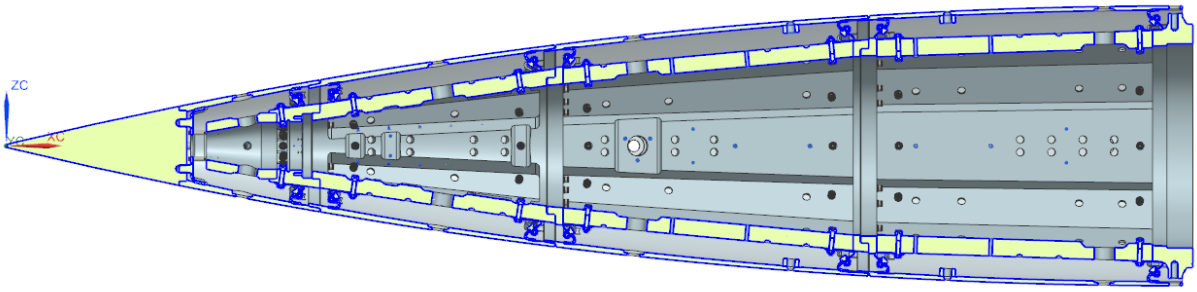

Fig. 5 STORT forebody overall cross section.

IV. Thermo-Mechanical Structure Validation

The ANSYS Mechanical software was employed to carry out numerical analyses of the forebody in order to support the design process and validate the overall resistance of the structure.

First an estimation of the thermal response of the CMC thermal protection system surface structures was obtained by an iterative procedure based on the general equation for the convective heat flux $\dot{q}_{conv}$, given by

$$\dot{q}_{conv} = \alpha(T_r - T_w)$$

where the heat transfer coefficient α was estimated with literature correlation equations [7] for the tip and the different segments, and the recovery temperature T_r was calculated based on the trajectory data. First, the convective heat flux was calculated for a cold wall condition and this value was used as input for the numerical simulation of the structures in the FEM code. The resulting wall temperatures were then taken to calculate again the convective flux as described and the new flux values were used to re-calculate the structure temperatures. This procedure was iterated until the change in the wall temperature of the structures was less than 5 %.

The transient heat flux profile together with the radiation energy emission of the body to the external environment was given as boundary condition for a transient thermal simulation. Fig. 6 shows the converged results in terms of convective heat flux and maximum wall temperature for each TPS segment. The results show that the heat load is significant, especially for the tip of the forebody, and that the resulting temperatures are high, which justifies the material choice.

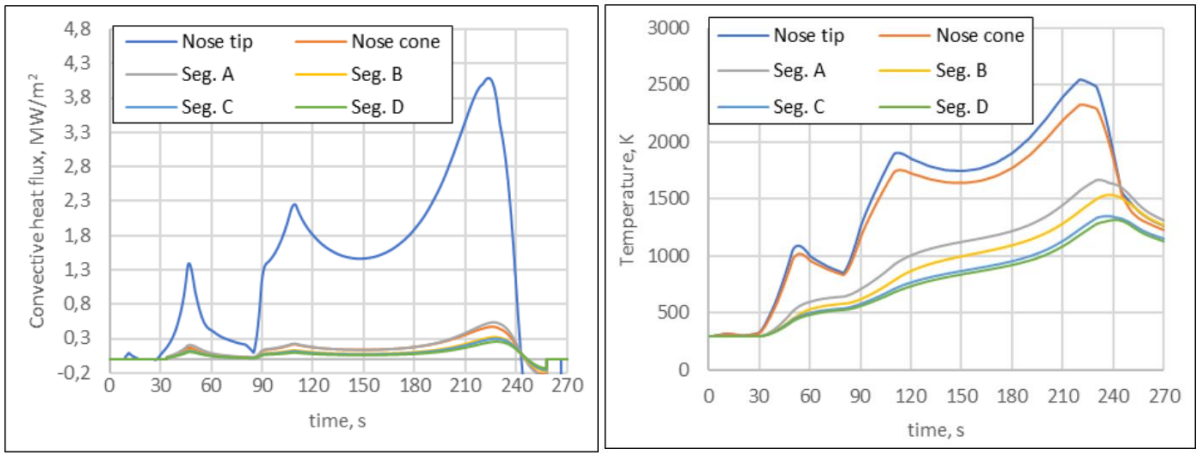

Fig. 6 Calculated maximum wall temperature and convective heat flux on the structure tip.

The maximum predicted heat flux on the stagnation point of the nose tip is at 4 MW/m² with a resulting temperature of roughly 2500 K. In the case of the shell segments, the loads are less severe, on the order of 0.5 MW/m², however, the temperatures are still in the range of 1700 K for the segment directly behind the nose tip.In the case of the nose tip, it was expected that during flight there would be some material recession due to oxidation as a result, however, as the flight time in the high-temperature regime is still quite short, the effect on the tip geometry with regard to the radius dimension and thus a reduction of the heat flux value was neglected. In Fig. 7 the temperature distribution over the external surfaces of the TPS shells and the tip is presented. It is noteworthy to see that due to the fact that the nose tip is a solid block of material, the temperature towards the end of the tip is considerably lower than the temperature of the following segment A which is a thin-walled shell.

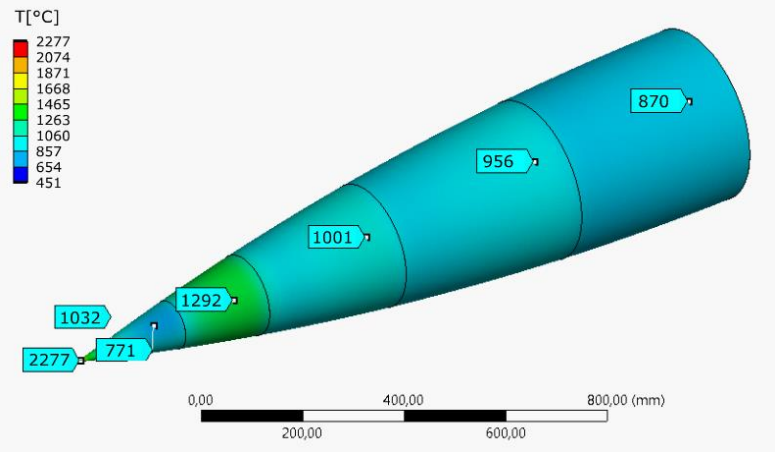

Fig. 7 Calculated temperatures on the TPS shells at t=230 s.

Considering the structural design process, the calculated temperatures were one major factor in the load environment as they lead to thermal expansion of the structures. The other relevant types of mechanical load are the aerodynamic pressure, the quasi-static acceleration from the increasing velocity of the launch vehicle and the accelerations from the motor vibration. Sound pressure variations from air turbulence are another factor, but difficult to estimate and thus not considered.

All these load types were investigated in more or less detail to validate the design against the predicted environment. The most critical elements in terms of structural performance were the mechanical connections between the hot CMC parts and the cold metallic structure underneath. The challenge was to find a design for these structural elements that allows for thermal expansion of the hot CMC shells while at the same time giving enough stability to support the aerodynamic pressure loads and the acceleration and vibration loads. A lengthy design process was carried out, investigating different design approaches, with the final design solution being the so-called double-l connection. A more detailed description of the methodology was given by Di Martino [8].

The double-l connection consists of two angled brackets that are roughly l-shaped. One of the brackets is also a CMC part and permanently joined to the CMC shell structure via the in-situ joining process, i.e. it is an integral part of the CMC shell structure after the CMC processing. The other part of the Double-L connection is a metallic part made from a high-temperature metal alloy, in this case Inconel 600. In Fig. 8 the schematic is presented in a semi-transparent view of the CMC shell segment B. The red components are the CMC L-brackets which are joined to the CMC shell. The yellow components are the metallic parts connected via bolts to both the understructure and the CMC brackets of the shell. The design proved to give the lowest stresses in the CMC part of the connection resulting from the thermo-mechanical loads while at the same time giving enough flexibility with regard to manufacturing and assembly tolerances.

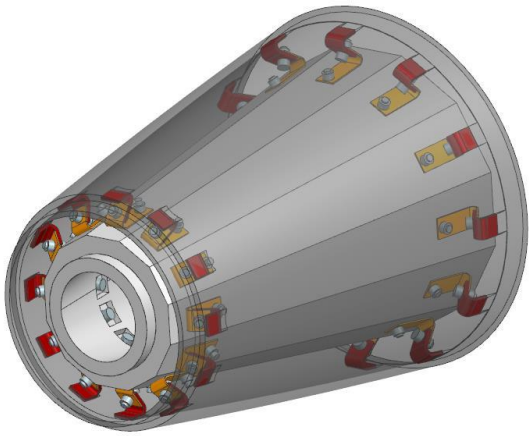

Fig. 8 Semi-transparent view of a CMC shell segment with one row of double-l connections at each end.

The resulting stresses CMC shells as well as in the components of the Double-L connections are presented for the case of the combined thermal and aerodynamic pressure load. The aerodynamic simulation of the STORT payload was carried out by the DLR Institute of Aerodynamics and Flow Technology (AS-HYP) to determine the aerodynamic load to which the structure is subjected in different points of the trajectory for different angles of attack. The most critical condition in terms of pressure load was determined to be at t=217.9 s at an angle of attack of 10°. The resulting pressure distribution is a roughly linear decrease from the tip to the end of the forebody as shown in Fig. 9.

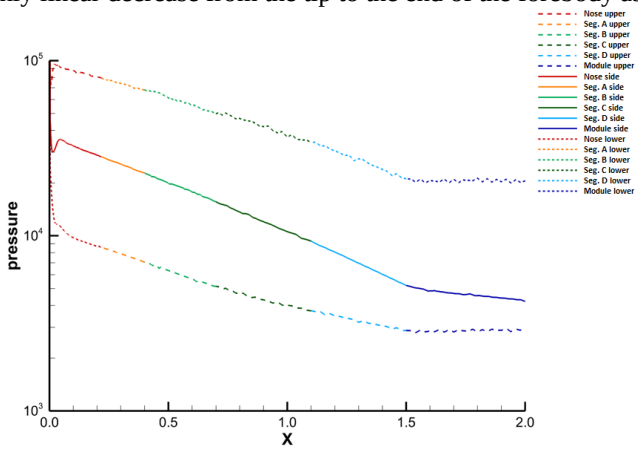

Fig. 9 Aerodynamic pressure distribution along the forebody at t_217.9 s at an angle of attack of 210°.

The pressure distribution was applied together with the temperature distribution over the individual segments. The segments were treated as independent from each other with regard to their mechanical behavior. The resulting total deformation is displayed for the segment B in Fig. 10. From the deformation plat it can be noted that the load case is not axisymmetric but due to the different pressure levels on the windward and leeward sides, the shell strucure is pushed upwards. This means that it is a complex case with the double-L connections partly in compression, some experience a tensile load case, while the ones on the sides are being twisted. Nevertheless, the stresses can be handled and are within acceptable limits. Table 1 shows the results of this most demanding load case for the four different segments.

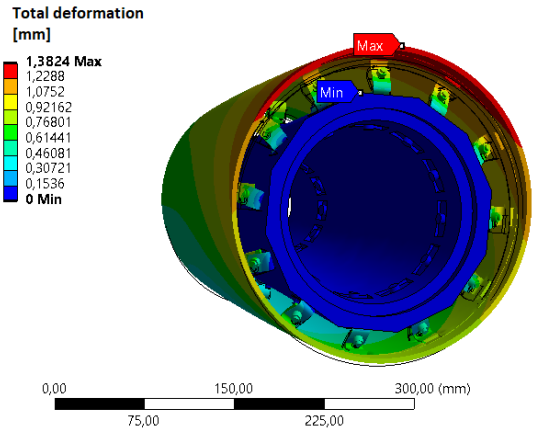

Fig. 10 Total deformation of segment B under combined load of aerodynamic pressure and temperature.

The results from the other load cases, as there are acceleration loads both in axial and transversal direction, have been presented already in detail [8]. Stresses are in general lower than in the combined pressure and temperature case presented above.

Table 1 Main results of the static mechanical simulation in the case of the critical aerodynamic pressure and thermal load at t=217.9 s

	Segment A	Segment B	Segment C	Segment D
Maximum axial displacement, mm	0.78	0.77	1.08	0.75
Maximum radial displacement, mm	0.57	1.25	1.68	0.96
Max. stress in CMC element, MPa	148.5	131.6	155.3	170.7
Av. shear stress at the joint surface, MPa	3.09	0.76	0.75	2.73

V. Hardware Manufacturing and Assembly

The CMC components of the forebody TPS were manufactured via in-house processes at the Institute of Structures and Design of DLR in Stuttgart. As mentioned, the design foresaw the use of axisymmetric shell segments, for which the manufacturing process consisted of the following steps.

- Manufacturing of the initial CFRP part via wet filament winding
- Pyrolysis process to create the C/C part
- In-situ joining of the connection elements in C/C-state
- Reactive melt infiltration with liquid silicon to create the C/C-SiC final component

The production process for the nose tip component was different because it was designed as a massive cone without internal hollow spaces. Three single plates of 30 mm thickness were produced and joined together. From the resulting plate of 90 mm thickness, the part was machined to the final contour and is shown in Fig. 11.

Fig. 11 STORT nose tip (not including boreholes for pressure and temperature measurements yet).

The production of the shell segments was more complex as indicated above. The sequence of the fabrication process is illustrated in the following images. Fig. 12 shows the wet filament winding of segment B, in the beginning of the winding procedure on the left, and the final, uncured CFRP component on the right.

Fig. 12 Wet filament winding of the shell segment B.

The components were subjected to the pyrolysis process after winding to convert the polymeric resin into carbon and create the typical crack pattern for the subsequent infiltration of liquid silicon. In Fig. 13 on the left hand side, the component after pyrolysis is shown. The machining of the shell segments to their final contour was also done mostly in the C/C condition to ease the process and reduce machining time. In Fig. 13 on the right, the machined component is displayed.

Fig. 13 Segment B C/C structure before (left) and after machining (right).

A major part in the shell strucure production was the intermediate in-situ joining process [6] of the attachment brackets on the front and rear ends of the shells. To this end, the wound shell structure itself was machined on the inside to create distinct joining areas where the brackets should be installed. The brackets were produced separately via the same processing route and cut to their final dimensions before joining. A dedicated joining device was used to carry out the actual joining procedure during which a specific mixture of polymeric resin and graphite powder is used as bonding agent. In Fig. 14 on the left, the prepared shell segment is shown, along with the CMC l-bracket in the joining fixture in the middle and on the right, the shell segment with 8 joining fixtures in position. The joining process had to be repeated three times per each edge of the shell to arrive at the full count of 12 brackets on each end.

Fig. 14 Internal view of the machined segment B with joining areas (left), C/C bracket in the joining device (middle), shell segment with four joining devices on each of end (right).

In the joining process, also a number of cylindrical seat parts for heat flux sensors were attached to the inside of the shells. The completed C/C components were then further processed via the reactive melt infiltration of liquid silicon in a high temperature furnace. The siliconized components only required minor additional machining work at the interfaces where two segments would meet and some cleaning at the contact surfaces of the attachment brackets as well as the preparation of installation grooves for thermocouple placement. In Fig. 15 an external view of the finished segment B component is shown on the left and a view of the inside with the attachment brackets and the sensor seats is given on the right. The production process of the other segments A, C and D was done in a similar way.

Fig. 15 STORT shell segment B in the final machined C/C-SiC condition (left); internal view on the in-situ joined CMC brackets and instrumentation reception points (right).

Each CMC shell segment of the forebody was assembled to its dedicated metallic structure assembly so that separate, fully assembled forebody segments were created. These were then stacked on top of each other and connected to assemble the full forebody. During the assembly process of the individual segments, the sensors were placed on the structures and a high temperature insulation was put in place between the metallic understructure and the CMC shell. The principle sequence of the assembly process is illustrated for segment D with the images in Fig. 16.

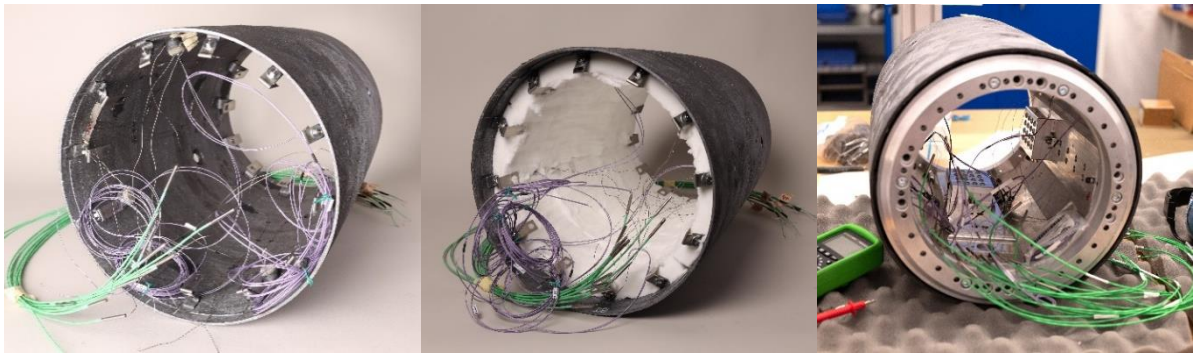

Fig. 16 Assembly sequence with sensor integration, insulation placement and metallic structure plus equipment integration, shown for the example of segment D.

The pre-assembled segments were finally stacked vertically and bolted together to arrive at the completed forebody as shown in Fig. 17. The assembled CMC forebody was taken for further integration to the premises of DLR-MRB in Oberpfaffenhofen. At DLR-MRB the CMC forebody was assembled to the other payload modules to arrive at the fully completed flight-ready STORT payload.

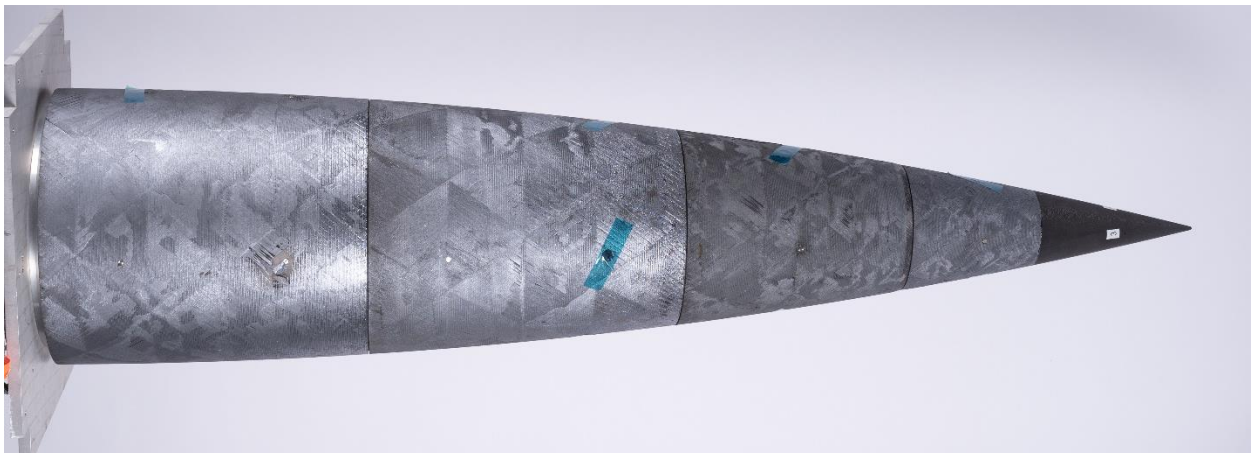

Fig. 17 Full assembly of the STORT CMC forebody.

Functional testing (bench tests) was carried out on the fully assembled STORT payload. The determination of physical properties like the measurement of the center of gravity and the inertia moments and the final environmental testing under vibration load was conducted at AIRBUS Munich. In Fig. 18 the complete STORT payload section is shown during the determination of inertia moments, giving also the descriptions of the other experimental and service modules of the payload.

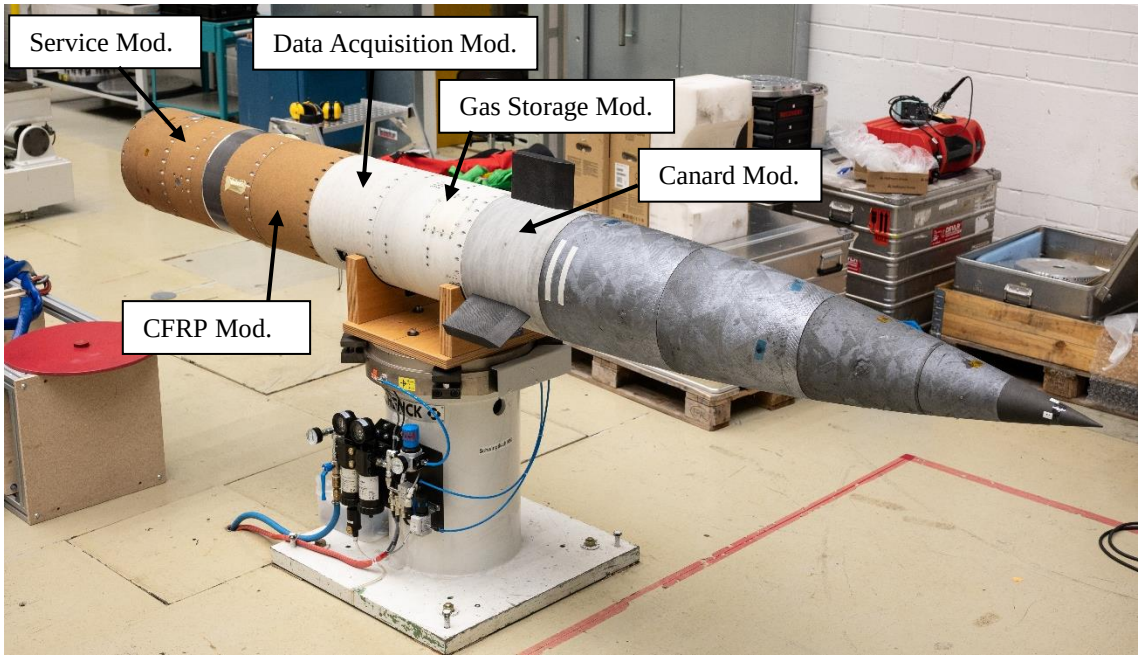

Fig. 18 STORT payload during determination of inertia moments.

The payload was equipped with a lot of instumentation. To this end the Service Module and the Data Acquistion Module served extremely important purposes by providing power to the equipment and collecting and transferring all the gathered data via telemetry downlink during flight. Apart from these service modules, there were two more payload modules which were of experimental character, the Canard Module and the Hybrid Module.

The CFRP Module shown in Fig. 19 served as an experiment to test new structure designs for application on sounding rockets or later on even bigger launchers. Traditionally the modules of the rocket are designed as cylindrical components made from aluminium material. In order to investigate the mass saving potential of advanced CFRP materials, the goal was to develop a structure module from a thermoplastic CF-PEEK mateial produced via AFP (Automated Fiber Placement) material which replaces one metallic module. In a previous flight experiment ATEK [9], the concept had been partially developed already, however, the interface flanges were still made from aluminium, only the cylindrical structure was made from CF-PEEK. In the STORT project, the complete structure including the interface flanges was built from CF-PEEK. Thereby the structure mass could be reduced from 5.8 kg (fully metallic) to 3.5 kg. In order to protect the CFRP structure from the heat loads during flight, the surface of the module was coated with a thin layer of cork thermal protection material.

Fig. 19 The CFRP-Module.

The Canard Module was an experiment dedicated to the topic of thermal management, both via active and passive cooling methods. There were three canard structures on the module. A different type of thermal management was applied to two of them while the third one served as a reference structure without thermal management applied. All

of the three canards were produced from CMC material. The first canard on the 60°-angle served as the reference component, built from standard material making use of PAN-based carbon fibers with no cooling. The second canard on the 180°-angle was built from C/C-SiC material using pitch-based fibers of a much higher thermal conductivity. The third canard on the 300°-angle was again built from standard material with standard fibers, but an internal active cooling system via impingement of a gas flow was installed, for which the gas was coming from the gas storage module behind the canard module. The angle is counted around the x-axis which points from the vehicle tip downstream as indicated in Fig. 20. Zero degree orientation is on the x-z-plane on the top of the vehicle.

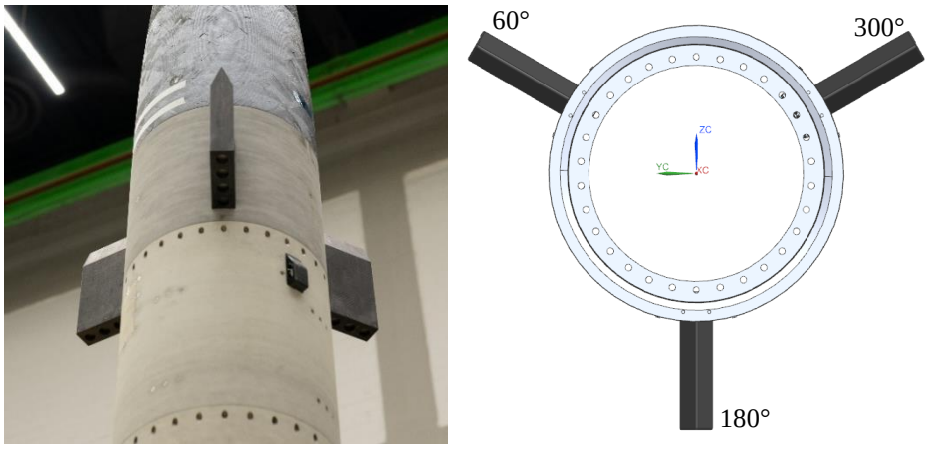

Fig. 20 Canard module assembled in the payload (left), overview sketch of the Canard Module (right).

In the canards, the leading edge was equipped with thermocouples at different heights. The sketch in Fig. 21 shows the installation positions.

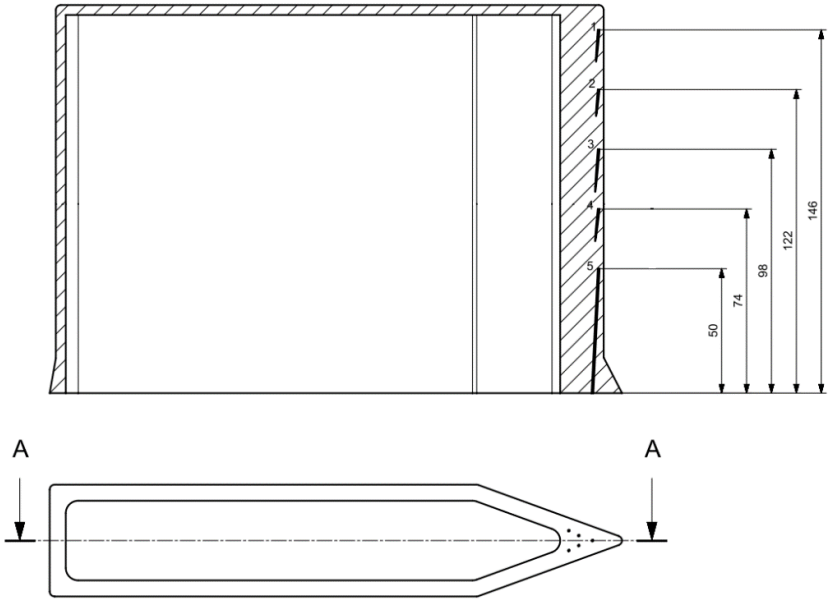

Fig. 21 Thermocouple installation positions in the canards.

VI. Testing

The environmental mechanical tests consisted of vibration tests of the full payload stack under a random vibration load. The main three axes of the vehicle were subjected individually to the vibration load.

Table 2 Load data for the environmental tests under vibration load.

		Axis		
		X	**Y**	**Z**
Sine Vibration				
Freq. Range	Hz	20-2000	20-2000	20-2000
Acceleration	g	0,25	0,25	0,25
Random Vibration				
Freq. Range	Hz	20-2000	20-2000	20-2000
ASD	g^2/Hz	0,051	0,029	0,029
RMS Acceleration	g	10	7,6	7,6
Peak Acceleration (3Sigma)	g	30	22,7	22,7

VII. Flight Results

The flight of the STORT experimental vehicle was successful. The suppressed trajectory was flown almost as planned with an apogee of 38 km compared to the target altitude of 45 km [4]. The duration of the flight velocity above Mach 8 was more than 60 seconds. All of the major engineering science experiements worked. The sensor data of the experiments and vehicle data could be transmitted via telemetry to the ground station until the vehicle was at a low altitude. The gives an overview about the main events of the flight. The reason for the slightly lower altitude was an error in the calibration during hardware-in-the-loop-tests. However, the Mach 8 velocity was reached as planned (although for a shorter time) and in fact at a lower altitude which means higher dynamic and aerothermal loads. So the STORT payloads were exposed to even more severe loads than anticipated. Fig. 22 shows the flown trajectory in comparison to the predicted one.

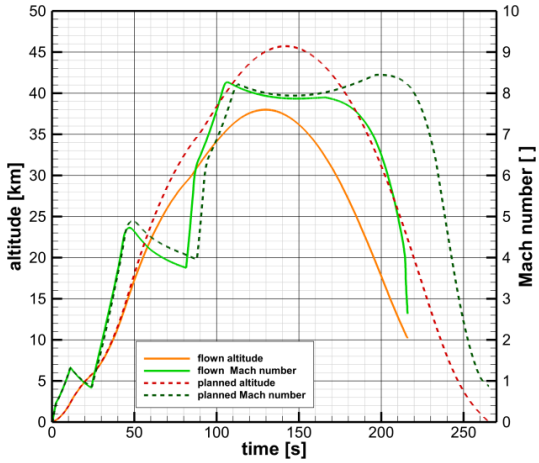

Fig. 22 STORT flown and predicted trajectory.

Table 3 Main events timeline during the STORT flight.

Event	Time s	Altitude km	Event	Time s	Altitude km
S30 Motor Ignition	0.00	0.04	S30 Motor Burnout	51.10	18.70
Launch Rail Exit	0.73	0.06	S30 Motor Separation, active	60.01	23.87
Spin Up Motor Ignition	0.84	0.07	IO Motor Ignition	88.00	34.69
Mach 1	8.39	1.45	IO Motor Burnout	113.00	42.08
S31 Motor Separation, passive	11.50	2.48	Apogee	141.90	45.73
S30 Motor Ignition	24.00	5.80	Impact	265.40	0.00

Maximum Dynamic Pressure	44.30	14.22	

From the perspective of the TPS development, the sensor data from the CMC forebody structures is the most interesting. Fig. 23 shows the position of the thermocouples installed in the CMC forebody together with their denominations except for the nose tip. The thermocouple positions in the nose are displayed in Fig. 24.

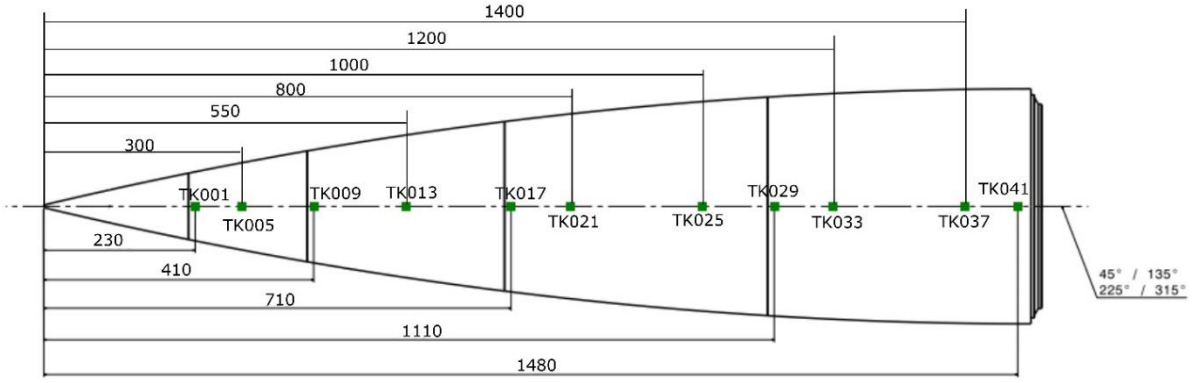

Fig. 23 Axial thermocouple positions on the STORT CMC forebody with name tag for the 45°-line. TCs were positioned on four lines from the stagnation point downstream separated by 90° angles.

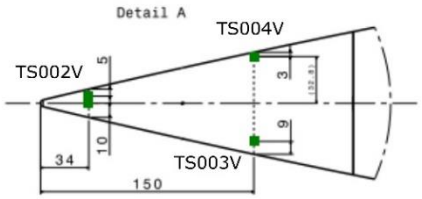

Fig. 24 Thermocouple positions in the STORT nose tip.

In Fig. 25 measured temperatures are shown for the CMC nose (left) and for the CMC segments A – D of the forebody in the case of the 45° line from stagnation downstream (right). The temperature of TS002V in the tip reaches 1111°C at 208.7 s and is the highest temperature measured on the tip and forebody except for the canards. The position of TS002V is the closest to the stagnation point as shown in Fig. 24 with a distance from 34 mm from the stagnation point and 5 mm to the outer surface in radial direction. The other two TCs TS003V and TS004V in the tip show considerably lower temperature values of 635.4°C at 214.9 s (still rising) and 701.1°C at 209.7 s, respectively, which is due to the fact that the tip is made from one massive block of material with more mass and thus heat capacity towards the end.

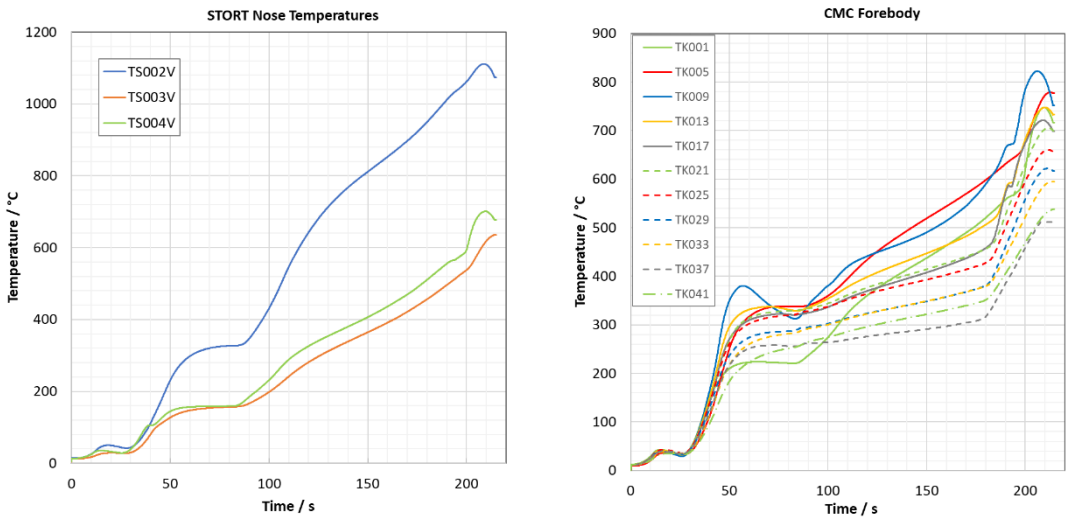

Fig. 25 Measured temperatures in the CMC nose tip (left) and on the 45° line over the forebody segments (right).

In Fig. 25 on the right, the temperatures of the forebody segments A-D on the 45°-line are shown. The different signals follow the general trend of decreasing temperature, the further downstream the measurement position is, except for TK001, which is the most forward thermocouple in segment A. After the burnout of the second stage it still shows the second lowest temperature of all positions at around 220°C, except for the TK0041 thermocouple which is the most backward of all positions on segment C. This is certainly due to the fact that it contacts the relatively cold end of the nose tip during the early phase of the flight and thus remains low in temperature. Over time, TK001 catches up and climbs to a temperature of 740°C towards the end of the flight, which is comparable to the other signals in that region.

A more detailed view on the flight data results of segment A is given in Fig. 26. It includes all sensors from all measurement planes and also for comparison the graphs of the numerical prediction for the position of the forward edge at 230 mm and the rear edge at 300 mm. It can be noted that the temperatures of the front edge are pretty close together, and the same can be said for the rear edge.

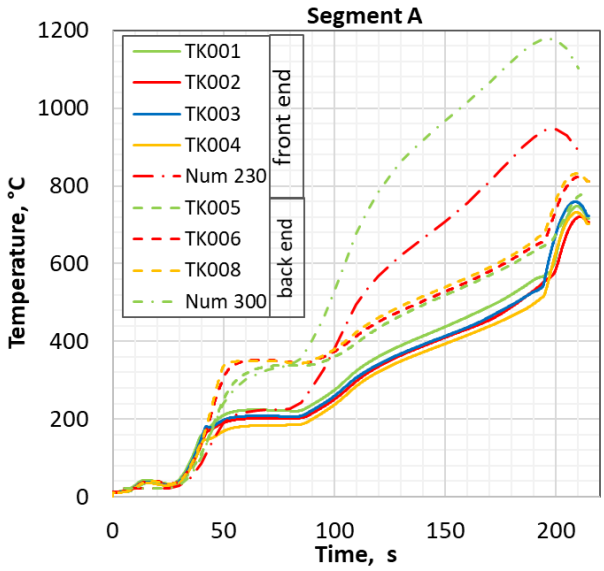

Fig. 26 Measured temperatures in the segment A on all measurement planes.

In Fig. 27 the measured temperatures in the canards are presented for all measurement positions for an overview on the left side. Solid lines are for the canard made from the reference material, dashed lines are the pitch fiber canard,

and dash-dotted lines are for the active cooling canard. It can be noted that most graphs are pretty close together and show a similar behavior in the temperature evolution over time except for the sensors that were located in the canard made of pitch fiber CMC material (TK064-TK068) which remain somewhat cooler at all times. A comparison between the three canard types focusing on just two TCs per canard is made on the right. There, the TCs closest to the foot (TK063, TK068 and TK073) and closest to the top (TK059, TK 064 and TK069) of the canard leading edges are compared. It can be noted that the pitch fiber canard (dashed lines) is showing the lowest temperature during the flight phase up to 120 s for both positions and for the low position up to the very end of the flight. If TK068 is compared to the corresponding TK063 and TK073, the temperature on the pitch fiber canard is roughly 300°C lower. In fact, the sensor TK068, the lowest TC on the pitch fiber canard survives until the very end of the flight, giving a maximum of 1323.8°C at 189.8 s. Just for information, the Mach number graph is included to show that the temperatures are very nicely following the condition of the flow velocity.

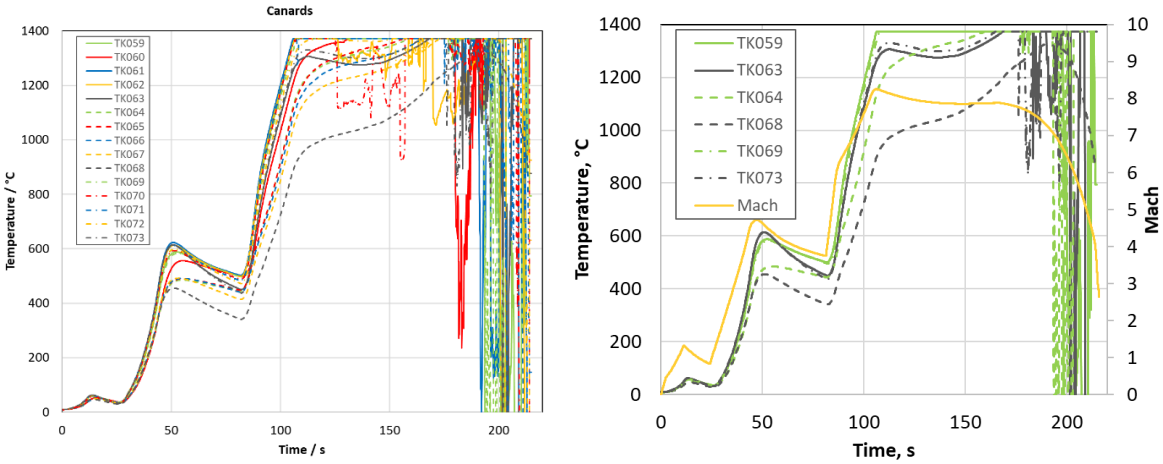

Fig. 27 Measured canard temperatures for all canards (left) and for the topmost and lowest TCs on each canard (right). Solid lines: reference material, dashed lines: pitch fiber, dash-dotted lines: active cooling.

From the point of view of the TPS to understructure connection, the double-l connection elements were of special interest with regard to their temperatures. During the design process, there was quite some discussion about what levels of temperature to be expected there, and if the metallic fasteners could handle the thermal environment. The temperatures at the double-l connection elements were measured in the segments B and C, which is shown in Fig. 28. The solid lines show the respective temperatures in the ceramic part of the connection, whereas the dashed lines show the temperatures in the metallic part. As it can be expecte the temperature in the ceramic part is higher and the temperature in the ceramic part of segment B is highe than the one in the ceramic part of segment C which is further downstream. In the ceramic part of the connection element in segment B, the temperature rises to just over 500°C towards the end of the flight, and in the ceramic part of segment C it goes up to roughly 370°C. For the metallic part of the connection, the maximum temperature in segment B is 300°C and for segment C it is 200°C.

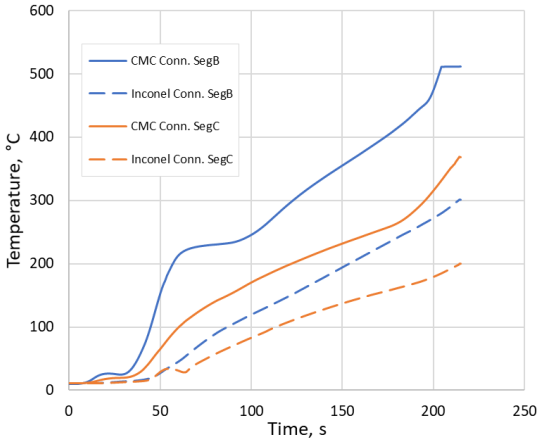

Fig. 28 Temperatures at the double-l connection elements in segments B and C.

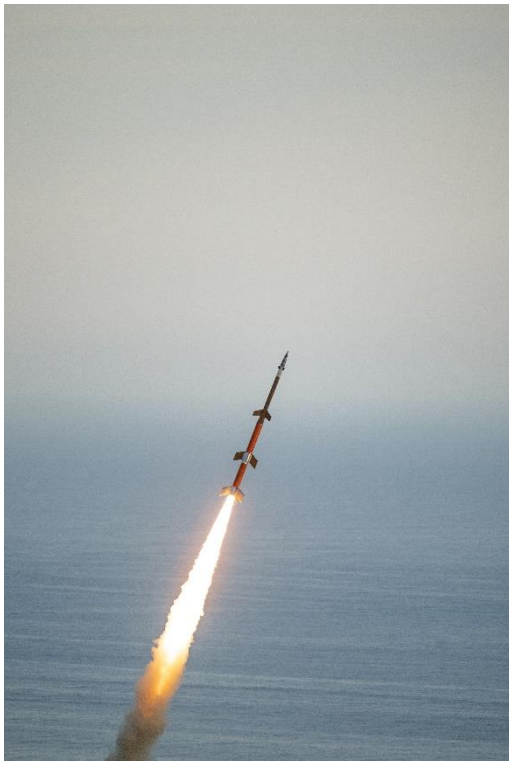

Fig. 29 Launch of the STORT flight experiment.

VIII. Conclusion

The experimental STORT flight was a great success. It was the first time that a three-stage sounding rocket system was designed and flown by DLR-MORABA. In particular in view of the ambitious suppressed trajectory at low altitude with the apogee of 38 km, this is of significance, because it gave the possibility to achieve an almost constant high Mach number of 8 for almost two minutes. Thereby, it was possible to collect relevant experimental data over an extended period of time in a demanding aerothermodynamic environment.

With regard to the structural development in the project, it could be shown that a hypersonic flight vehicle could be designed, of which the forebody surface is fully made from CMC structures. That was essential, because as a consequence of the extended flight time at high Mach number it was expected that the vehicle would get quite hot all over. The CMC structures were designed as circumferentially closed, axial-symmetric, thin-walled shell structures to avoid as much as possible flow perturbations. Because they were thin-walled shell structures, they had to be treated as hot structures due to the extended flight time, which resulted in a high temperature of the complete shell structure. In order to compensate for the differential thermal expansion between the hot CMC structures and the cold metallic structure, while at the same time to guarantee mechanical stability of the overall structural system, a lot of work was invested in the design of a suitable connection between the CMC shell structures and the metallic understructure. A favourable solution was found by designing a connection that consists of two l-shaped components, one of which is an integral part of the CMC shell, whereas the other is made from a high-temperature metallic alloy and connects to the internal metallic structure. The specific geometries of both components allow for enough flexibility – coming mainly from the metallic part – to compensate for the thermal expansion mismatch and at the same time provide enough stability to bear the mechanical loads from pressure and vibration.

In terms of the CMC production process, it could be shown that the C/C-SiC shell segments could be produced very well by wet filament winding and that by employing the in-situ joining process for the CMC parts of the connection elements, complex integral structures could be produced in order to fulfill the mechanical and aerodynamic requirements.

A very interesting experimental structure was the CFRP module inserted between service module and data acquisition module. It showed that the standard metallic launcher structures can be replaced by composite structures

which save on the order of 40 % of the mass, while maintaining stiffness and strength. For a system as the described STORT payload on top of the third stage, this means that a mass saving of roughly 10 kg is possible if the CFRP technology is applied to the other modules as well. This might not seem a lot, especially when considering the issue that quite often ballast mass is used to adjust CoG, however, this can make the difference between adding one more large experiment or not, at least in terms of mass.

The Canard module provided for some interesting data concerning the flow around aerodynamic surfaces which are thermally highly loaded. More specific data on the related experiments like shock-shock interaction and boundary transition will be presented by the colleagues from the AS-HYP department in DLR Cologne. Because of problems with the cooling gas supply system and very low nitrogen mass flow rate, the efficiency of the internal gas impingement cooling could not be verified. In contrast, the effect of the pitch-fiber CMC material on the temperature distribution is significant. Due to the large in-plane thermal conductivity of the material, the leading edge temperature could be reduced significantly by approximately 300°C when similar measurement positions are compared.

The forebody of the vehicle was equipped with a lot of instrumentation, including thermocouples, heat flux gauges and pressure sensors. A great amount of data was collected during the flight. The detailed evaluation of the flight data is ongoing and will still take some time, but first indications are that the data is as expected. It has to be mentioned that the telemetry data transmission from the vehicle to the ground station worked fine up to a late time in the flight, so that data could be collected also after the nominal end of the flight down to an altitude of roughly 10 km.

The measured peak temperature in the nose tip was 1111°C. For the segments A-D the peak temperatures were 778°C, 822°C, 721° and 621°C respectively. The temperatures seem not to be too high at first glance but this has to be seen in perspective. First, the temperature of the nose was measured at a distance of 34 mm behind the actual tip in a region where the temperature gradients are huge. When the measured temperature is compared to the prediction for the position, the difference is small, so it can be assumed that also the tip temperature itself was roughly as predicted at 2200°C. Moreover, even though the flight time was relatively long in comparison to previous hypersonic flight experiments, it has to be noted that the conditions were not steady-state yet. There was still significant increase in the temperatures almost everywhere on the vehicle with the exception of a few positions on the canards. This means that in steady-state conditions the temperatures would indeed be still higher.

The last issue is also the motivation for considering yet longer flight times at such conditions to finally achieve a situation which is corresponding to steady-state flight. This would require potentially different or more powerful motors for first and second stage to arrive earlier at the desired conditions and then to have a third stage which just keeps up the speed and continues for as long as possible.

In any case, the presented work is a strong argument for the validity of hypersonic flight research on sounding rockets. The ratio between cost and achieved results is extremely favourable, as well as the relatively short cycles between flights so that fast gains can be achieved in the technology.

Acknowledgments

The support of the workshop and technical staff at the Institute is greatly acknowledged which was of great help to produce and assemble the hardware in time for the flight. The authors wish to thank especially Felix Vogel from the CMC department and Frank Entenmann from Space System Integration for their support.

References

[1] Weihs, H., Longo, J., Turner, J., "The Sharp Edge Flight Experiment SHEFEX II, a Mission Overview and Status," *15th AIAA International Space Planes and Hypersonic Systems and Technologies Conference*, AIAA, 2008-2542, 2008
doi: 10.2514/6.2008-2542

[2] Bauer, W., "DLR Reusability Flight Experiment ReFEx," Acta Astronautica, 168, 57-68 (2019)
DOI: 10.1016/j.actaastro.2019.11.034

[3] Dumont, E., Ishimoto, S., Tatiossian, P., Klevanski, J., Reimann, B., Ecker, T., Witte, L., Riehmer, J., Sagliano, M., Giagkozoglou, S., Petkov, I., Rotärmel, W., Schwarz, R., Seelbinder, D., Markgraf, M., Sommer, J., Pfau, D., Martens, H., "CALLISTO: A Demonstrator for Reusable Launcher Key Technologies," *Transactions of the Japan Society for Aeronautical and Space Sciences*, Aerospace Technology Japan, 19 (1), 2021

[4] A. Gülhan, D. Hargarten, M. Zurkaulen, F. Klingenberg, F. Siebe, G. di Martino, T. Reimer; "*Objectives and Achievements of the Hypersonic Flight Experiment STORT*", IAC-22, Paris, 18-22 September 2022, IAC-22, D2,6,7,x69473

[5] Krenkel, W., in “Ceramic Matrix Composites: Fiber Reinforced Ceramics and their Applications,” Wiley & Sons, 2008, ISBN 3527622403
[6] R. Kochendorfer, N. Lutzenburger, H. Weihs, Joining Techniques for Fibre Ceramic Structures, *Advanced Composites Letters*, 13 (1) (2004)
doi: 10.1177/096369350401300106
[7] Van Driest, E.R., The Problem of Aerodynamic Heating, Aeronaut. Eng. Review, Vol. 15 No. 10, 1956.
[8] Di Martino, G.D., Reimer, T., Dauth, L., Baier, L., Structure Design of a Sounding Rocket Fairing with a Segmented Filament Winding-Ceramic Matrix Composite Thermal Protection System, HiSST: 2nd International Conference on High-Speed Vehicle Science Technology, 11–15 September 2022, Bruges, Belgium
[9] Gülhan, A., Siebe, F., Klingenberg, F., Kallenbach, A., Petkov, I., “Main Achievements of the Sounding Rocket Flight Experiment ATEK,” *72nd International Astronautical Congress*, IAC, IAC-21, D2-6.4, x62713, 2021